Journal of Anatomy

J. Anat. (2015) **227**, pp89–102 doi: 10.1111/joa.12333

Changes in gene expression and cell shape characterise stages of epibranchial placode-derived neuron maturation in the chick

Alexandra C. Smith, Stephen J. Fleenor and Jo Begbie

Department of Physiology, Anatomy and Genetics, University of Oxford, Oxford, UK

Abstract

Sensory neurons in the head are largely generated from neurogenic placodes. Previous studies have revealed early events in placode development; however, the process of maturation has not been studied. In this study, it has been shown that placodal neurogenesis follows a sequential progression with distinct stages defined by expression of specific markers. These markers highlight domains of maturation within the stream of migratory neuroblasts that extend between the placode and the neural tube. Commitment to neurogenesis occurs in the apical placode, with the newborn neuroblasts delaminating basally and entering a transition zone. The neuroblasts migrate through the transition zone, differentiating further and becoming post-mitotic as they approach the ganglionic anlage. It has further been demonstrated that this progression from the transition zone to the ganglionic anlage is accompanied by a switch from multipolar to bipolar cell morphology. This sequential progression parallels events observed elsewhere in the nervous system, but here the stages are distinct and anatomically segregated. It is proposed that placodal neurogenesis provides a tractable system to examine the transition between states in neurogenesis.

Key words: chick; epibranchial; neurogenesis; placode; sensory.

Introduction

In the vertebrate head the majority of sensory neurons are derived from specialised regions of ectoderm called neurogenic placodes (Blentic et al. 2011; Begbie, 2013). It has traditionally been suggested that the mechanism of placode-derived sensory neurogenesis is likely to mirror the production of neural crest-derived sensory neurons in the trunk. Indeed, in both cases there are parallels in cellular behaviour such as delamination and migration, and shared expression of some of the key genes. As the specific process is studied in more depth in each population, however, it is becoming apparent that there are significant differences, especially in timing.

In the trunk, sensory neurons are derived exclusively from neural crest cells (NCCs). NCCs delaminate from the dorsal aspect of the neural tube (NT) by epithelial-to-mesenchymal transition and remain as NCCs as they migrate along a defined ventromedial pathway to the site of dorsal root ganglion (DRG) formation (George et al. 2010). With the arrival of NCC at the site of DRG formation, a small number of cells begin to differentiate as sensory neurons. These neurons then act to nucleate the ganglion with the developing DRG consisting of a neuronal core enclosed within a perimeter of proliferating progenitors. These progenitors are derived from later waves of migrating NCCs and will go on to differentiate as sensory neurons contributing to the expanding core (George et al. 2010). Analysis of the genetic control of sensory neurogenesis in NCCs shows that expression of the transcription factors *Ngn1* and *Ngn2* in NCCs is required in their specification as sensory neurons (Parras et al. 2002; Marmigere & Ernfors, 2007). Subsequently, the neuronal precursors within the prospective ganglion differentiate further, upregulating neuronal genes such as *Brn3a* and *Isl1*, and sensory neuron-specific genes such as *Foxs1* in the mouse and *Hmx1* in the chick (Marmigere & Ernfors, 2007; Adameyko et al. 2009).

In the head, sensory neurons derive from two cell populations, with the majority derived from the neurogenic placodes and to a lesser extent from the cranial NCCs (D'Amico-Martel & Noden, 1983). The neurogenic placodes are specialised regions of neurogenic epithelium found in stereotypical locations across the cranial ectoderm (Ladher et al. 2010). In the chick, the neurogenic placodes comprise the two separate trigeminal placodes, ophthalmic and

Correspondence
Jo Begbie, Department of Physiology, Anatomy and Genetics, University of Oxford, South Parks Road, Oxford OX1 3QX, UK.
T: +44 1865 282832; F: +44 1865 272420; E: jo.begbie@dpag.ox.ac.uk

Accepted for publication *29 April 2015*
Article published online *17 June 2015*

maxillomandibular, generating neurons of the respective lobes of the trigeminal ganglion; the otic placode, producing neurons of the vestibuloacoustic ganglion; and the three epibranchial placodes, which give rise to the geniculate, petrosal and nodose ganglia (Fig. 1A). Each of the neurogenic placodes generates neurons in its own way, and this study focuses on the epibranchial placodes (Begbie et al. 2002; Alsina et al. 2004; McCabe et al. 2009; Blentic et al. 2011). Previous research has shown that all placode-derived neurons are specified within the placodal epithelium, and are consequently already neuronal when they delaminate from the epithelium and migrate towards the site of ganglion formation (Abu-Elmagd et al. 2001; Begbie et al. 2002; Lassiter et al. 2014). This is in contrast to the NCC-derived sensory neurons that are formed at the site of ganglion formation (George et al. 2010). In the case of the epibranchial and trigeminal maxillomandibular placodes, these cells are neuroblasts that can proliferate as they migrate but are post-mitotic within the ganglion (Blentic et al. 2011).

It was hypothesised that the advance in maturity of placodal neuroblasts as they migrate further away from the placode and closer to their target destination in the ganglion may be reflected by the molecular identity of the cells and thus expression of typically neuron-associated genes. To address this, the expression of a panel of well-characterised neuronal and neurogenic markers within the migratory stream across three stages of placode-derived cranial sensory ganglion (CSG) development has been examined (Fig. 1B). A number of these markers have been used in studies focused on early stages of epibranchial placodal neurogenesis: *Ngn1, NeuroD, NeuroM* (Abu-Elmagd et al. 2001), and *Delta1, Phox2a, Phox2b, Isl1* (Begbie et al. 2002). The panel also included a variety of transcription factors associated with neuronal differentiation: *MyT1* (Matsushita et al. 2002), *COE1* (Garcia-Dominguez et al. 2003), *Foxg1* (Hatini et al. 1999) and *DRG11* (Rebelo et al. 2007). To characterise later stages of neuronal maturation, known markers of mature neurons and genes involved in cellular processes such as neuronal migration and axon guidance were selected: HuC/D (Blentic et al. 2011), NFM (Perrot et al. 2008), *SCG10* (Groves et al. 1995), *Axonin1* (Ratie et al. 2014) and *DCX* (Capes-Davis et al. 2005). Here it is reported that using these markers, the migratory stream can be subdivided into four domains of increasing maturity.

It was hypothesised that within the domains of maturation there would also be a transition point in cell shape as neuroblasts begin to establish adult neuron morphological characteristics such as axonal processes (Neukirchen & Bradke, 2011). To address this, GFP-labelling was used to analyse neuroblast cell shape within the migratory stream. Here it is reported that a switch from multipolar to bipolar cell morphology within the final domain of gene expression corresponding to the ganglionic anlage can be defined. The results show that neuronal maturation during epibranchial ganglion development shows a sequential progression, with distinct stages showing a clear anatomical segregation.

Materials and methods

Embryos

Fertilised hen's eggs from Winter Egg Farm (Hertfordshire, UK) were incubated horizontally at 38 °C in a humidified incubator to the relevant developmental stages (HH; Hamburger & Hamilton, 1992). Embryos were harvested and fixed in MEMFA (0.1 M MOPS, 2 mM EGTA, 1 mM $MgSO_4$, 3.7% formaldehyde) overnight at 4 °C.

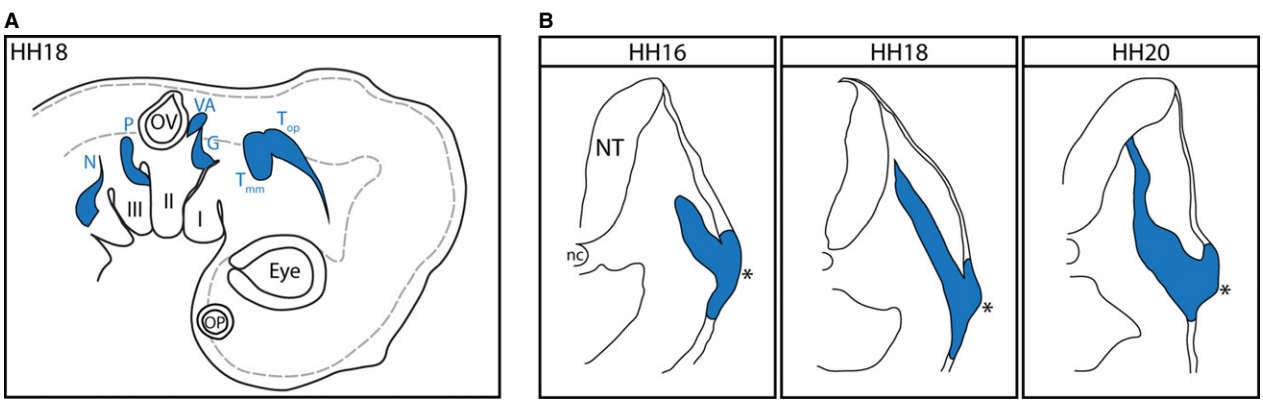

Fig. 1 The CSG form at stereotypic positions in the embryo. (A) Schematic side view of a day 3 chick embryo showing the positions of the CSG, as well as the olfactory, lens and otic placodes. I–III, branchial arches 1–3; G, geniculate; N, nodose; nc, notochord; NT, neural tube; OP, olfactory placode; OV, otic vesicle; P, petrosal; T_{mm}, trigeminal maxillomandibular; T_{op}, trigeminal ophthalmic; VA, vestibuloacoustic. The NT is outlined by the grey dashed line. (B) The distal CSG form by internal migration of neuroblasts derived from the placodal ectoderm. The shape of the migratory stream undergoes characteristic changes as development progresses culminating in the aggregation of neuronal cell bodies to form the ganglion proper. The asterisk indicates the placodal epithelium.

In situ and immunohistochemistry

In situ hybridisation was carried out as described (Thompson et al. 2010). cDNA constructs for preparing riboprobes were *Axonin1* (E Stoeckli, Zurich); *Cad7, COE1, Isl1, Delta1, Foxg1* (A. Graham, KCL); *DRG11* (J. Cohen, KCL); *HMX1* (P. Ernsfors, Stockholm); *NeuroD* (B. Alsina, Barcelona); *NeuroM* (P. Scotting, Nottingham); *Ngn1* (M. Ballivet, Geneva); *Phox2a, Phox2b* (JF. Brunet, Paris). *MyT1* was an EST, chEST738o2, from ARK-genomics (Boardman et al. 2002). Polymerase chain reaction was used to clone *DCX* using forward primer: TGGAAGCATGGATGAGCTGG and reverse primer: CAGTCCC CAATCTCCACACC; and *Tbr2* using forward primer: GCTTTTGCAA AGGGCTTCAGA and reverse primer: CTGGATAGAGACTCCGCCCT; both cloned from HH18 chick cDNA.

Immunohistochemistry was carried out as described (Thompson et al. 2010).

Antibody	Ig	Animal	Manufacturer	Cat. no.	Concentration
Primary antibodies					
GFP	G	Rabbit	Life Technologies	A11122	1 : 500
HuC/D	G	Mouse	Life Technologies	A-21271	1 : 500
NFM	G	Mouse	Life Technologies	RMO-270	1 : 5000
NFM	G	Rabbit	Abcam (Cambridge, UK)	ab9034	1 : 500
Secondary antibodies					
Alexa-488 rat	G	Goat	Life Technologies	A11006	1 : 1000
Alexa-488 rabbit	G	Goat	Life Technologies	A11008	1 : 1000
Alexa-555 mouse	G	Donkey	Life Technologies	A31570	1 : 1000
Alexa-568 mouse	G	Goat	Life Technologies	A11004	1 : 1000
Alexa-647 rabbit	G	Donkey	Life Technologies	A31573	1 : 1000

GFP placodal labelling (electroporation)

Embryos (HH11–13) were electroporated *in ovo* with four 10-V pulses at 5 ms each, using a BTX® Electro Square Porator™ ECM830. DNA was injected into the albumen surrounding the branchial arch region using a pulled glass capillary needle and electrodes positioned either side of the embryo. Eggs were then resealed and incubated for a further 26–28 h to HH17–18. A combination of cytoplasmic GFP and GPI-anchored GFP was used to ensure total cell labelling (both at 2 $\mu g\ \mu L^{-1}$). DNA was prepared for injection with 0.05% Fast Green dye and 0.01% carboxymethyl cellulose (provided by Dr C. Patthey, Umeå; Graham et al. 2007).

Imaging

Brightfield and epifluorescence imaging were carried out using an Olympus BX51 compound light microscope connected to a Lumen 200 Fluorescence Illumination System (Prior Scientific, Cambridge, UK). Brightfield images were acquired using differential interference contrast.

High-resolution imaging of transverse sections of electroporated embryos was carried out using a Zeiss LSM710 confocal microscope at $\times$ 20 and $\times$ 40 magnification.

Quantification

Measurements of marker expression were carried out on transverse sections from three separate embryos at each of the three stages analysed, for each gene. These measurements are presented as the percentage of the total migratory distance at which expression begins and ends, given as the mean $\pm$ SEM%.

Analysis of migratory neuroblast morphology was carried out by tracing three cells of each of the two morphological types from Z-stacks generated from three separate GFP-electroporated embryos.

Results

Measuring the migratory neuroblast stream from the petrosal placode

To document the maturation of placode-born neurons, expression patterns for a panel of neurogenic markers were determined by *in situ* hybridisation or immunofluorescence at stages HH16, HH18 and HH20 of chick embryo development. Of the three epibranchial placodes, all of which generate neurons in a similar manner, the petrosal placode (Fig. 1A) was chosen as the one most suitable for generating consistent data across samples. The petrosal placode generates a defined stream of migratory neuroblasts originating from a clearly identifiable placodal thickening, and the neuroblasts follow a reasonably straight trajectory and do not have to navigate other neuronal structures such as the developing vestibuloacoustic ganglion in the case of geniculate placode-derived neuroblasts (Fig. 1B). The developmental stages analysed fall within the window of neurogenesis for the petrosal placode, which begins at HH14 and ends at HH24 (Blentic et al. 2011), and as such represent early placodal neurogenesis, the peak of neuroblast migration and early ganglion aggregation.

A systematic method of analysis was established that allowed accurate determination of the position at which marker expression begins and ends within the migratory stream, measured in transverse sections through the pharyngeal region of each stained embryo (Fig. 2). This distance was expressed as a percentage of the total distance separating the apical edge of the placode and the predicted entry point of neuroblast projections into the NT. The positions were determined by placing a grid of 20 concentric semi-circles onto an image of a transverse section of a stained embryo at the level of the petrosal placode. The central point of the grid was set on the middle of the outer (apical) surface of the placodal ectoderm and

the outermost circle set to intersect the NT at the predicted axonal entry point (Fig. 2A). Thus, each arc of the grid represents 5% of the full length of the migratory path, and the two arcs flanking its proximal and distal limits can define the extent of gene expression. In each case, three specimens were analysed and the data presented in graphical form to represent the localisation of gene expression within the migratory stream (Fig. 2B).

To localise the axon entry/exit point at the NT, expression of *Cad7*, known to be expressed by a sub-population of NCCs that surround the prospective exit point of the cranial branchiomotor axons, was analysed (Niederlander & Lumsden, 1996). Transverse sections through HH16, 18 and 20 embryos at the level of rhombomere 6 (r6) showed that the entry/exit point was positioned just ventral to the point at which the dorsal NT bends outward, forming a slight kink (arrowhead, Fig. 2B). This was used as an anatomical landmark to position the grid, defining the end point of the migratory stream.

Delta1, *Ngn1*, *NeuroD*, *NeuroM* and *Isl1* are expressed from the apical surface of the placode

Delta1

Previous studies have shown that the placode is a pseudostratified epithelium (Graham et al. 2007). The expression of *Delta1* expression was seen at the apical surface of the placodal ectoderm: $0 \pm 0\%$ of the migratory stream (Fig. 3A; $n = 3$ for each stage). The expression was restricted to the placodal ectoderm with an internal limit seen at $11.67 \pm 0.96\%$ at both HH16 and HH18 (Fig. 3Ai,ii), and at $10 \pm 0\%$ at HH20 (Fig. 3Aiii).

Ngn1

As seen for *Delta1*, *Ngn1* expression was detected at the apical surface of the placodal epithelium, beginning at $0 \pm 0\%$ of the migratory stream at all stages analysed (Fig. 3B). The internal limit of expression extended further at each sequential stage ($11.67 \pm 0.96\%$ at HH16, $18.33 \pm 096\%$ at HH18, and $20 \pm 0\%$ at HH20), unlike *Delta1* (Fig. 3B).

NeuroD and NeuroM

As previous studies have suggested that there is a temporal difference between the onset of *NeuroM* expression and that of *NeuroD* (Abu-Elmagd et al. 2001), both were examined.

NeuroD expression was detected at the apical surface of the placode, falling within the first 5% of the migratory stream at all stages analysed ($3.33 \pm 0.96\%$ at HH16, $0 \pm 0\%$ at HH18 and $1.67 \pm 0.96\%$ at HH20; Fig. 3C). The internal limit of expression in the migratory stream was

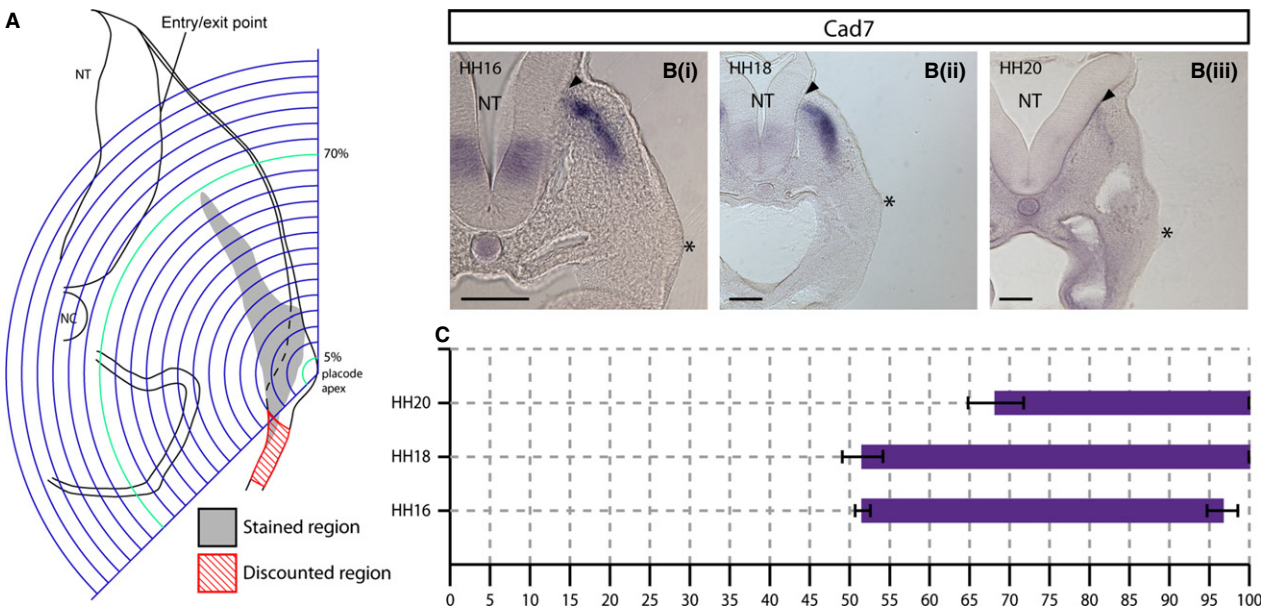

Fig. 2 Expression analysis schematic and analysis of expression of the neural tube (NT) entry/exit point marker *Cad7*. (A) Schematic representation of a transverse section of a HH18 embryo at the level of the petrosal placode. Concentric arcs are centred on the apex of the placodal ectoderm and are scaled so that the outermost arc intersects the basal surface of the NT at the predicted entry/exit point of sensory/motor axons (blue). Staining extending ventrally within the placodal ectoderm was discounted for this analysis (red hatched region) as the focus was on the changes in gene expression in the axis of migration. The extent of staining was defined by the arcs flanking the proximal and distal limits of the observed labelled region (green). NC, notochord. (Bi–iii). *In situ* hybridisation showing *Cad7* expression in transverse sections at the level of the petrosal placode at (i) HH16, (ii) HH18 and (iii) HH20. *Cad7* is expressed in a population of NCCs surrounding the predicted entry point of sensory axons into the NT (arrowheads) and extend towards the placode. (C) Graphical representation of *Cad7* expression where the *x*-axis = distance from placode to NT as a percentage. $N = 3$ for each stage. Error bars = SEM. Scale bars: 100 μm. The asterisk indicates the placodal epithelium.

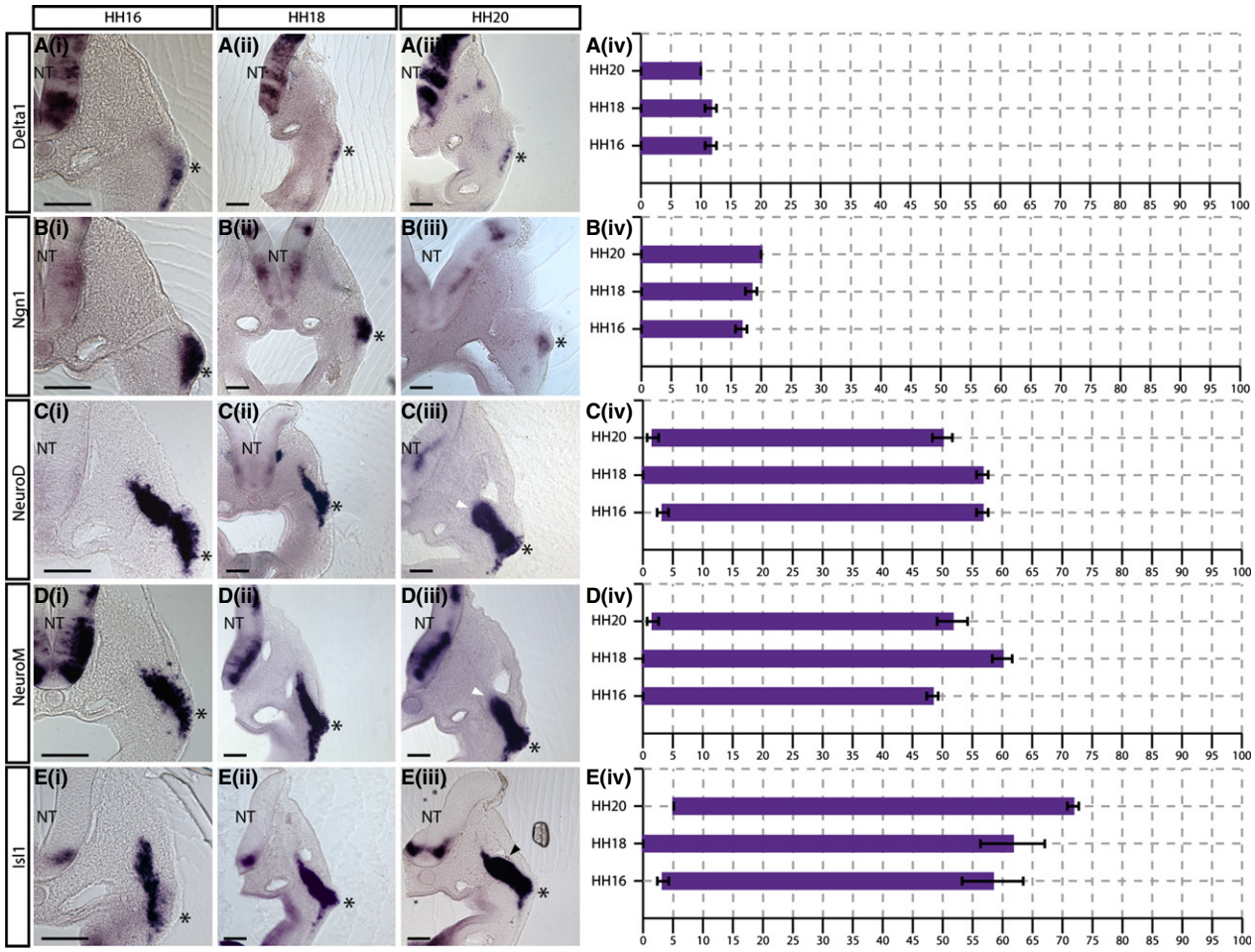

Fig. 3 *Delta1*, *Ngn1, NeuroD, NeuroM* and *Isl1* are expressed from the apical border of the placodal ectoderm. (i–iii) *In situ* hybridisation showing (A) *Delta1*, (B) *Ngn1*, (C) *NeuroD*, (D) *NeuroM* and (E) *Isl1* expression in transverse sections at the level of the petrosal ganglion at (i) HH16, (ii) HH18 and (iii) HH20. The asterisk indicates the placodal epithelium. The shape of the migratory stream changes at HH20, forming a characteristic swelling at the site of the prospective ganglion [arrowheads in (iii)]. The expression of *NeuroD* and *NeuroM* clearly demarcates the internal limit of the ganglionic anlage (white arrowheads in Ciii and Diii). (iv) Graphical representations of expression patterns where the *x*-axis = distance from placode to neural tube (NT) as a percentage. $N = 3$ for each stage. Error bars = SEM. Scale bars: 100 μm.

56.67 ± 0.96% at HH16 and HH18 (Fig. 3Ci,ii). Unlike many of the other markers analysed in this study, *NeuroD* expression did not extend further dorsally at later stages and the internal limit was found to be 50 ± 1.67% at HH20 (white arrowhead, Fig. 3Ciii).

The pattern of *NeuroM* expression in transverse sections closely resembled that of *NeuroD*. *NeuroM* was expressed from 0 ± 0% of the migratory stream at HH16 and HH18, and 1.67 ± 0.96% at HH20 (Fig. 3D). The internal limit of *NeuroM* expression was 48.33 ± 0.96% at HH16; 60 ± 1.67% at HH18, and 51.67 ± 2.54% at HH20, suggesting that it extends furthest towards the NT at HH18 and is then refined (white arrowhead, Fig. 3D).

Isl1

Isl1 expression was detected at the apical surface of the placodal epithelium, 3.33 ± 0.96% at HH16, 0 ± 0% at HH18, and 5 ± 0% at HH20 (Fig. 3E). The internal limit of expression extended further towards the NT at each successive stage analysed (58.33 ± 5.09% at HH16, 61.67 ± 5.36% at HH18, and 71.67 ± 0.96% at HH20; Fig. 3E). The ganglionic anlage could be clearly seen as a swelling within the migratory stream at HH20 (arrowhead in Fig. 3Eiii).

Comparison of the graphs showed that *Delta1, Ngn1, NeuroD, NeuroM* and *Isl1* expression was detected from the apical surface of the placodal epithelium, suggesting that they are among the first genes to be switched on, and that neuronal differentiation begins in the apical placode (Fig. 3A–Eiv). There was, however, divergence between the expression patterns at their internal limit. *Delta1* and *Ngn1* expression were restricted to the pseudostratified placodal epithelium, with both being expressed apically but Ngn1 extending further internally than Delta1 (Fig. 3A,B). This suggests that

Ngn1 expression is maintained in neuroblasts that translocate basally within the epithelium. *NeuroD, NeuroM* and *Isl1* expression extended into the migratory stream, suggesting they are expressed in neuroblasts that have exited the placodal ectoderm and begun to migrate internally (Fig. 3C–E). Interestingly, *NeuroD* and *NeuroM* expression showed an internal limit at the ganglionic anlage, while *Isl1* expression extended beyond it towards the NT (Fig. 3C–E).

Foxg1, Phox2a, Phox2b and NFM are excluded from the apical region of the placodal epithelium

Foxg1

The expression of *Foxg1* was detected from $5 \pm 0\%$ of the placode–NT distance, at all stages analysed (Fig. 4A). This corresponds to the basal region of the placodal ectoderm, in contrast to the markers described in the apical region in the previous section. The internal limit of *Foxg1* expression was found to extend further at each sequential developmental stage analysed ($43.33 \pm 0.96\%$ at HH16, $58.33 \pm 3.47\%$ at HH18, and $66.67 \pm 3.47\%$ at HH20; Fig. 4A).

Phox2a and 2b

Like *Foxg1, Phox2a* and *2b* expression were detected from $5 \pm 0\%$ in the placodal epithelium (Fig. 4B). The internal limit of *Phox2a* expression was seen at $48.33 \pm 0.96\%$ of the stream at HH16, and 66.67 ± 0.96 at HH18 (Fig. 4Bi,ii). This internal limit was then reduced to $63.33 \pm 3.47\%$ at HH20 with staining extending beyond the swelling of the ganglionic anlage, but appearing to refine towards it (arrowhead in Fig. 4B).

Unlike *Phox2a*, the internal limit of *Phox2b* expression extended further dorsally at each successive stage analysed ($51.67 \pm 1.92\%$ at HH16; $73.33 \pm 1.92\%$ at HH18; and $85 \pm 1.67\%$ at HH20; Fig. 4C). While expression was strong within the ganglionic anlage at HH20, a significant number of positive cells were observed closer to the NT (Fig. 4C).

NFM

NFM protein expression was analysed by immunofluorescence. Transverse sections revealed an interesting feature of NFM staining in the epibranchial placodes whereby two types of staining were apparent: in regions distant from the placode, staining appeared as long filamentous

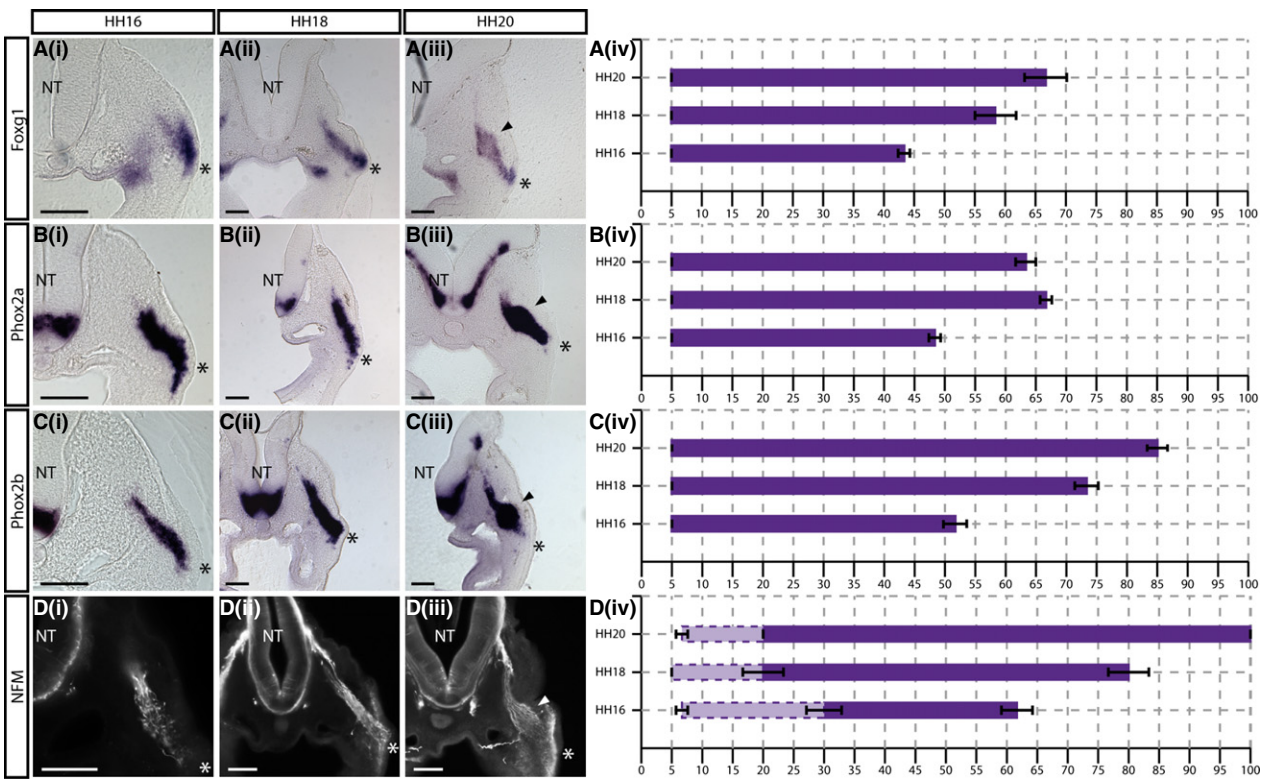

Fig. 4 *Foxg1, Phox2a, Phox2b* and NFM expression begins more basally within the placodal ectoderm. (i–iii) *In situ* hybridisation showing (A) *Foxg1*, (B) *Phox2a* and (C) *Phox2b*, and immunostaining showing (D) NFM expression in transverse sections at the level of the petrosal ganglion at (i) HH16, (ii) HH18 and (iii) HH20. Arrowheads indicate ganglionic anlage. (iv) Graphical representations of expression patterns where the *x*-axis = distance from placode to neural tube (NT) as a percentage. NFM staining appears fragmented in regions close to the placode (lighter purple, dotted lines), while further from the placode, NFM staining appears filamentous, labelling cells and neuronal processes as they extend towards the NT (purple, solid lines). $N = 3$ for each stage. Error bars = SEM. Scale bars: 100 μm. The asterisk indicates the placodal epithelium.

structures extending towards the NT along the axis of migration; while, in regions adjacent to the placode, staining appeared more fragmented. Fragmented staining consistently began within the first 10% of the migratory stream, corresponding to the basal region of the placodal ectoderm ($6.67 \pm 0.96\%$ at HH16, 5% at HH18, and $6.67 \pm 0.96\%$ at HH20; Fig. 4D). Organised filamentous staining appeared more internally within the migratory stream ($30 \pm 2.88\%$ at HH16, $20 \pm 1.67\%$ at HH18, and $20 \pm 0\%$ at HH20; Fig. 4D). The internal limit of NFM staining extended further towards the NT at each successive stage, eventually reaching the entry point at the NT: $61.67 \pm 2.55\%$ at HH16, $80 \pm 1.67\%$ at HH18, and $100 \pm 0\%$ at HH20 (Fig. 4Div).

Comparison of the graphs showed that *Foxg1, Phox2a, Phox2b* and NFM expression was excluded from the apical-most region of the placodal epithelium with staining detected from approximately 5% of the total migratory distance at all stages (Fig. 4A–Div). Thus, these markers reveal a next step in neurogenesis, labelling neuroblasts as they move into the basal region of the placodal epithelium and delaminate.

MyT1, Axonin1, DRG11, COE1 and *DCX* are upregulated in neuroblasts migrating away from the placode

MyT1

Analysis of *MyT1* expression showed that staining was seen from $8.33 \pm 0.96\%$ of the migratory stream at HH16, $10 \pm 0\%$ at HH18, and $13.33 \pm 0.96\%$ at HH20 (Fig. 5A). The internal limit of *MyT1* expression was seen at $45 \pm 1.67\%$ at HH16, then at $70 \pm 1.67\%$ at HH18 (Fig. 5Ai,ii). This limit was not found to be substantially more internal at HH20, reaching a maximum of $71.67 \pm 3.85\%$ (Fig. 5Aiii).

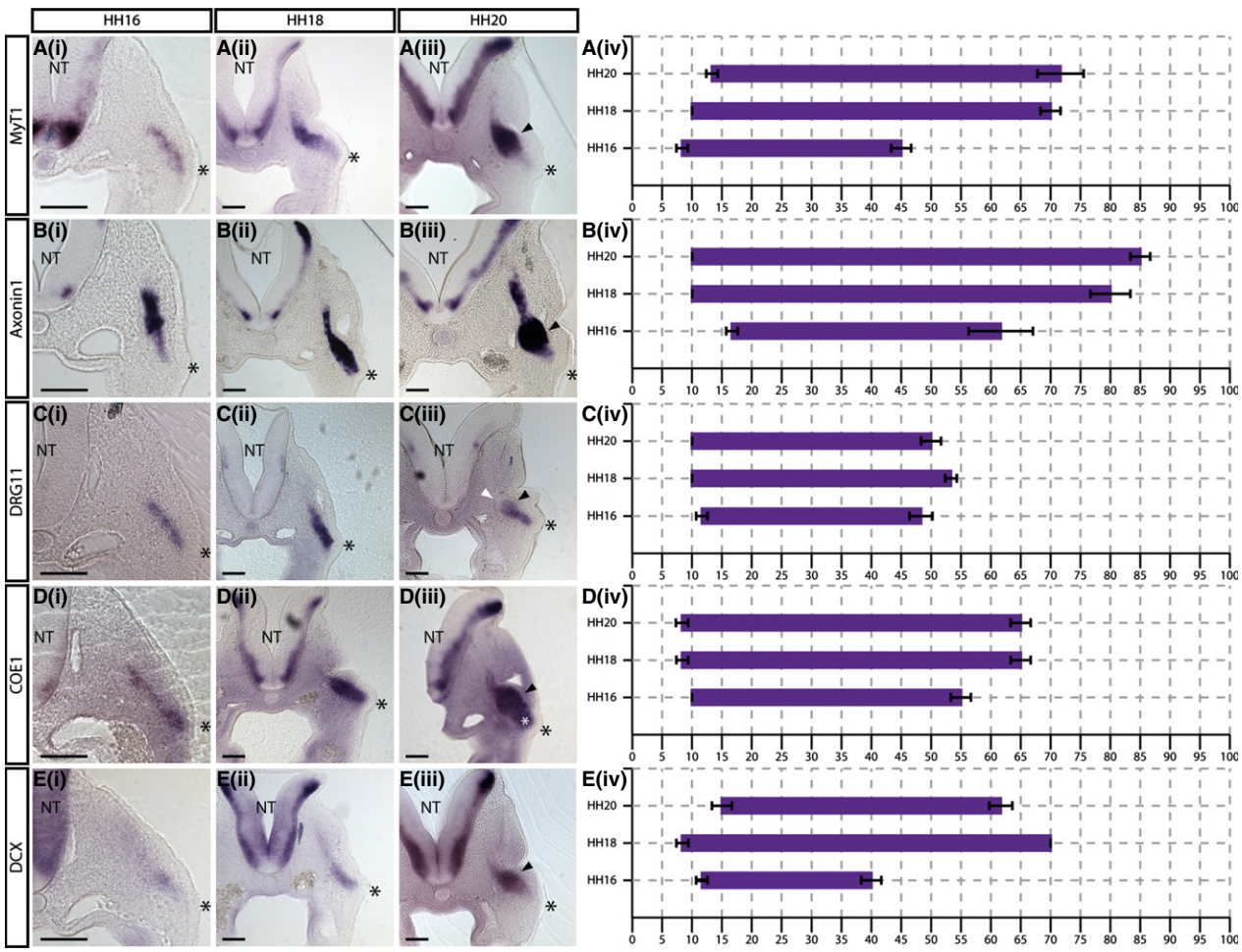

Fig. 5 *MyT1, Axonin1, DRG11, COE1* and *DCX* expression is excluded from the placodal ectoderm. (i–iii) *In situ* hybridisation showing (A) *MyT1*, (B) *Axonin1*, (C) *DRG11*, (D) *COE1* and (E) *DCX* expression in transverse sections at the level of the petrosal ganglion at (i) HH16, (ii) HH18 and (iii) HH20. Black arrowheads indicate ganglionic anlage. Expression of *DRG11* clearly demarcates the internal limit of the ganglionic anlage (white arrowhead in Ciii). (iv) Graphical representations of expression patterns where the *x*-axis = distance from placode to neural tube (NT) as a percentage. $N = 3$ for each stage. Error bars = SEM. Scale bars: 100 μm. The asterisk indicates the placodal epithelium.

Axonin1

The expression of *Axonin1* (*Contactin2, TAG1*) was seen from 16.67 ± 0.96% of the total placode–NT distance at HH16 (Fig. 5Bi) while, at later stages, staining was seen closer to the placode, starting at 10 ± 0% of this distance at HH18 and HH20 (Fig. 5Bii,iii). The internal limit of *Axonin1* expression was seen progressively closer to the NT with development: at HH16, staining extends to 61.67 ± 5.36% of the total migratory path, and to 80 ± 3.33% and 85 ± 1.67% at HH18 and HH20, respectively (Fig. 5B).

DRG11

DRG11 expression was detected directly adjacent to the basal region of the placodal epithelium at all stages analysed: 11.67 ± 0.96% at HH16 (Fig. 5Bi), and 10 ± 0% at both HH18 and HH20 (Fig. 5Bii,iii). The internal limit of the staining was found to be approximately 50% of the placode–NT distance at all stages (48.33 ± 1.92% at HH16, 53.33 ± 0.96% at HH18, 50 ± 1.67% at HH20; Fig. 5B). This is similar to the patterns observed for *NeuroD* and *NeuroM* (Fig. 3C,D). It was noticeable that the level of *DRG11* expression was lower and appeared to be in a smaller number of cells than *NeuroD* and *NeuroM,* suggesting that DRG11 may label a subset of the migrating neuroblasts.

COE1

Analysis of *COE1* (*EBF1*) expression showed that staining was seen from 10 ± 0% of the migratory stream at HH16 (Fig. 5Ci), and from 8.33 ± 0.96% at both HH18 and HH20 (Fig. 5Cii,iii). The internal limit was found to be 55 ± 1.67% at HH16, and 61 ± 1.67% at HH18 and HH20 (Fig. 5C). Interestingly, at HH20, the region of the migratory stream just internal to the placode is broader than other members of this group (white asterisk, Fig. 5iii).

DCX

The expression of *DCX* was detected from 11.67 ± 0.96% of the migratory stream at HH16, 8.33 ± 0.96% at HH18, and 15 ± 0.67% at HH20 (Fig. 5D). The staining for *DCX* was weak at HH16 and the internal limit was determined to be 40 ± 1.67% (Fig. 5Di). In comparison, robust *DCX* labelling was apparent from HH18, and extended to 70 ± 0% of the distance (Fig. 5Dii). At HH20, the internal limit was 61 ± 1.92%, with expression appearing to refine towards the ganglionic anlage (white arrowhead, Fig. 5Diii).

Comparison of the graphs showed that *MyT1, Axonin1, DRG11, COE1* and *DCX* expression was excluded from cells within the placodal epithelium, with staining seen from about 10% of the total migratory distance (Fig. 5A–Div). It is suggested that these genes are upregulated as neuroblasts migrate away from the placode. The markers were expressed throughout the migratory stream, but interestingly display variable internal limits of expression.

HuC/D and *SCG10* are upregulated at a distance from the placode

HuC/D

Analysis of transverse sections of immunostained embryos shows that HuC/D staining was only seen in cells that have migrated a significant distance from the placode. Staining was first detected at about 20% of the total migratory stream at all stages (20 ± 1.67% at HH16, 20 ± 0% at HH18, and 20 ± 1.67% at HH20; Fig. 6A). The internal limit of HuC/D-positive cells was 71.67 ± 3.47% at HH16, 81.67 ± 2.55% at HH18, and 81.67 ± 0.96% at HH20 (Fig. 6A).

SCG10

SCG10 expression closely followed the pattern observed for HuC/D expression. Like HuC/D, staining for *SCG10* began at 20 ± 0% of the migratory stream at HH16 (Fig. 6Bi). This onset was somewhat shifted towards the placode at later stages, being 18.33 ± 0.96% at HH18 and 16.67 ± 1.92% at HH20, but still remained well removed from the basal surface of the placodal ectoderm (Fig. 6Bii,iii). The internal limit of *SCG10* expression within the migratory stream was 52.5 ± 3.54% of the migratory stream at HH16, then reaching 80 ± 1.67% at HH18 and 81.67 ± 2.55% at HH20 (Fig. 6B).

Comparison of the graphs for these markers showed that HuC/D and *SCG10* expression was first detected at about 20% of the migratory stream (Fig. 6Aiv,Biv), suggesting that these markers come on in neuroblasts that have reached the ganglionic anlage.

HMX1 implicated in sensory neuron development in the trunk is not expressed in the migratory stream

HMX1 has been previously shown to play a role in specifying sensory neurons in the trunk DRG (Adameyko et al. 2009). In the present study, it was found that *HMX1* was strongly expressed in the otic vesicle and developing eye at all stages analysed (Fig. 6C), however it was not expressed in epibranchial neurons at HH16 and HH18 (asterisk in Fig. 6Ci,ii). At HH20, additional regions of strong expression were apparent in the posterior aspect of the second branchial arch, and in a region extending along the rostro-caudal axis ventral to the developing trigeminal ganglion and dorsal to the first branchial arch (bracket, Fig. 6Ciii). The latter region of staining extends a little over the pharyngeal pouch separating the first and second branchial arches and transverse sections at this stage suggesting there may be some weak expression in the geniculate placode (arrowhead, Fig. 6Ciii), but not in the migrating neuroblasts. *HMX1* expression was not detected in the petrosal and nodose placodes at any of the stages analysed.

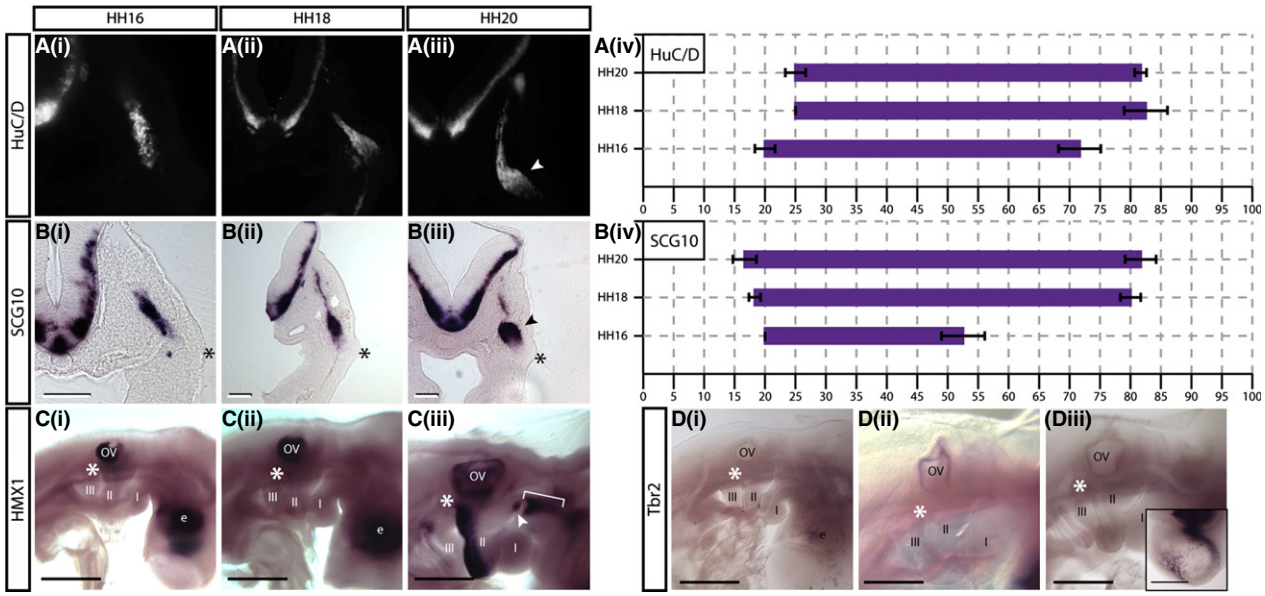

Fig. 6 (A, B) *SCG10* and HuC/D are expressed only in cells having reached the site of ganglion aggregation. (i–iii) *In situ* hybridisation showing (A) *SCG10*, and immunostaining showing (B) HuC/D expression in transverse sections at the level of the petrosal ganglion at (i) HH16, (ii) HH18 and (iii) HH20. Arrowheads indicate ganglionic anlage. (iv) Graphical representations of expression patterns where the *x*-axis = distance from placode to NT as a percentage. $N = 3$ for each stage. Error bars = SEM. (C, D) Lateral view of *in situ* hybridisation showing (C) *HMX1* and (D) *Tbr2* in whole embryos at (i) HH16, (ii) HH18 and (iii) HH20. *HMX1*, a sensory marker in DRG, is absent from the petrosal placode and neurons (C, asterisk). It is expressed in the otic vesicle (OV) and developing eye (E) at all stages examined. At HH20, *HMX1* expression is seen in the posterior aspect of the second branchial arch, and a region in the first branchial arch (bracket) that extends to the geniculate placode at HH20 (Ciii, arrowhead). *Tbr2*, a marker of intermediate progenitors in the cortex, is not expressed in the petrosal placode or neurons (D, asterisk). *Tbr2* expression is detected in the telencephalon (inset in Diii). $N = 3$ for each stage. Scale bars: 500 μm.

Dividing neuroblasts do not express *Tbr2,* a marker of intermediate progenitors in the cortex

Previous studies have shown that some of the placodal neuroblasts are able to divide away from the apical surface of the placodal ectoderm after delamination (Begbie et al. 2002; Blentic et al. 2011). This led to the hypothesis that they may resemble the intermediate progenitors of the cortex in marker expression. Therefore, the marker of cortical intermediate neuronal progenitors, *Tbr2*, was included in the present panel (Englund et al. 2005; Sessa et al. 2010). Analysis of whole-mount *Tbr2 in situ* hybridisation showed that expression was very specific with positive cells detected in the developing forebrain from HH16 onwards (Fig. 6D). The number of cells expressing *Tbr2* increased with development, and could be seen broadly distributed through the forebrain at HH20 (see inset Fig. 6Diii). However, at all stages analysed *Tbr2* expression was completely absent from any of the cranial placodes or developing CSG (asterisks in Fig. 6D).

Morphology of neuroblasts changes through the migratory stream

The gene expression patterns described above delineate four distinct regions arranged sequentially along the placodal neuroblast migratory stream. These data support the hypothesis that the placodal cells progress along the neuronal differentiation pathway as they migrate from their origin, maturing as they reach the site of ganglion formation. In order to assess maturation by a parameter other than gene expression, it was examined whether the placodal cells underwent morphological changes at distinct points in the migratory stream. Changes in neuronal morphology during neuronal differentiation have been well described in the CNS where cells initially exhibit a multipolar morphology before undergoing a switch to a bipolar morphology with the selection of an axon (Tabata et al. 2009; Neukirchen & Bradke, 2011; Kitazawa et al. 2014).

To analyse cell morphology, confocal Z-stacks of 100-μm transverse sections encompassing the petrosal placode level of GFP–placode electroporated HH18 embryos were generated. It has previously been shown that GFP electroporation into the placode at HH12 results in specifically labelled migrating placodal neuroblasts (Graham et al. 2007). The initial qualitative evaluation of these confocal data revealed that two principal types of cell morphology were present within the migratory stream: multipolar and bipolar cells (Fig. 7A).

To further characterise these morphology types, three representative cells from each category in three separate embryo samples were traced (i.e. $N = 9$). Typically,

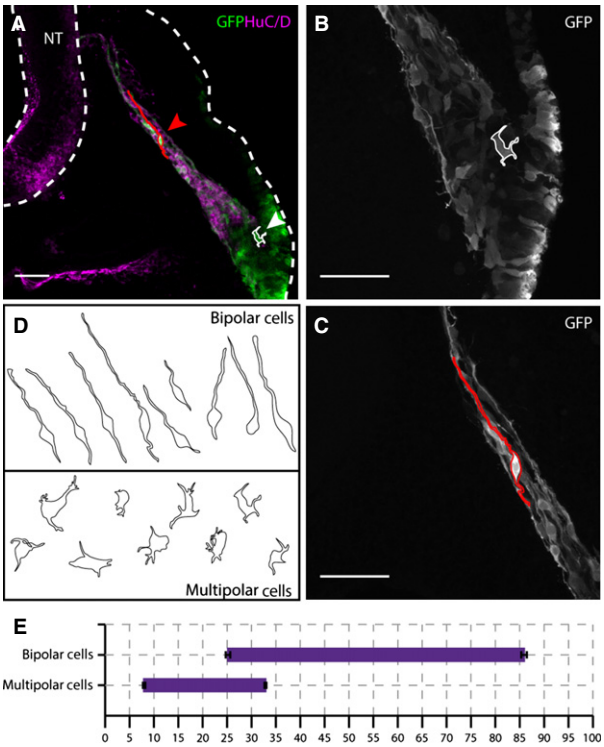

Fig. 7 Placode-derived neuroblasts adopt two different types of morphology after delamination from the placode, dependent on their position within the migratory stream. (A) Flattened × 20 confocal stack of a transverse section through the petrosal ganglion of a HH18 embryo, co-electroporated with cyt-GFP and GPI-GFP (green) and immunostained for HuC/D (magenta). White cell outline of a representative trace of a multipolar cell (white arrowhead) is located close to the placodal ectoderm, in the HuC/D-negative region. Red cell outline of a representative bipolar cell (red arrowhead) is located more internally, in the HuC/D-positive region. Dashed white line outlines the neural tube (NT) and outer perimeter of the embryo. (B, C) Higher-magnification confocal image (× 40) of the cells outlined in (A). (B) Multipolar cell located directly adjacent to the placodal epithelium and characterised by several short processes extending from an irregularly shaped cell body. (C) Bipolar cell located distant from the placodal ectoderm and characterised by a long leading process extending towards the NT and a compact, rounded cell body. (D) Summary of bipolar and multipolar cell traces. $N = 9$ cells of each morphology (= 3 cells × 3 embryos). (E) Graphical representation of the distribution of the two types of morphology at HH18, *x*-axis = distance from placode to NT as a percentage. Error bars = SEM. Scale bars: 50 μm.

multipolar cells had a broad, amorphous cell body with short processes projecting in multiple directions, with no obvious alignment to the axis of migration (Fig. 7B–D). In contrast, bipolar cells had small, condensed and rounded cell bodies from which one leading and one trailing process extended. The projections of the bipolar cells were always aligned to the axis of migration, with the leading process extending towards the NT and the trailing process extending towards the placode. The trailing process was found to be significantly shorter than the leading process, and was absent in some cases (Fig. 7B–D).

The qualitative analysis suggested that the two cell types were found predominantly in spatially distinct regions of the migratory stream. The multipolar cells were seen as part of a large, disorganised cohort immediately adjacent to the placodal ectoderm (Fig. 7A,B). Bipolar cells were identified some distance away from the placode (Fig. 7A,B), often with the cell bodies forming small clusters from which leading processes extend in tight bundles. In some instances, the bipolar cell leading processes were found to make contact with the NT, and even extend further within the neuroepithelium, perpendicular to the apico-basal axis. This second morphological type was thus clearly associated with more mature neurons.

To be able to compare the morphological changes with the changes in gene expression, the method described previously was used to determine specific positions along the migratory stream (Fig. 2A). Distances were measured between the apical surface of the placode and the first and last observable cell body of each morphological type for three independent samples. The analysis showed that multipolar cells were first seen at $8 \pm 0.2\%$ of the total migratory distance, while the last was seen at $32.86 \pm 0.25\%$. In contrast, the bipolar cells were first seen at $25.18 \pm 0.47\%$ of the migratory stream, indicating that there is a small region of the stream in which both types of morphology are intermingled, while the last bipolar cell was seen at $85.88 \pm 0.56\%$.

Discussion

It is becoming clear that the way that sensory neurons are generated from neurogenic placodes in the head is different from their generation by NCCs in the trunk. While the early stages of placode induction and neuronal fate commitment have been well studied, the molecular and cellular basis of later stages of placode-derived neuron maturation is not so well characterised in the context of the epibranchial ganglia. To address this issue, the aim was to categorise expression of neurogenesis-related genes along the axis of inwards neuroblast migration across three developmental stages (Figs 1 and 2). To correlate molecular with cellular maturation, detailed analysis of GFP-labelled neuroblast cell morphology at HH18 was carried out (Fig. 7).

A method of analysis was devised that allowed accurate determination of the points within the migratory path of petrosal placode-derived neuroblasts at which expression of each marker begins and ends (Fig. 2). This analysis was carried out for 16 neurogenesis-related markers (Figs 3–6). The summary of combined expression patterns showed that these markers can be divided into four categories based on the region of the migratory stream in which they are upregulated (Fig. 8). The data suggest that each of the four groups of genes is upregulated sequentially as the neuroblasts migrate away from the placode. It was suggested that these four domains of expression correspond to distinct phases of neuronal maturation:

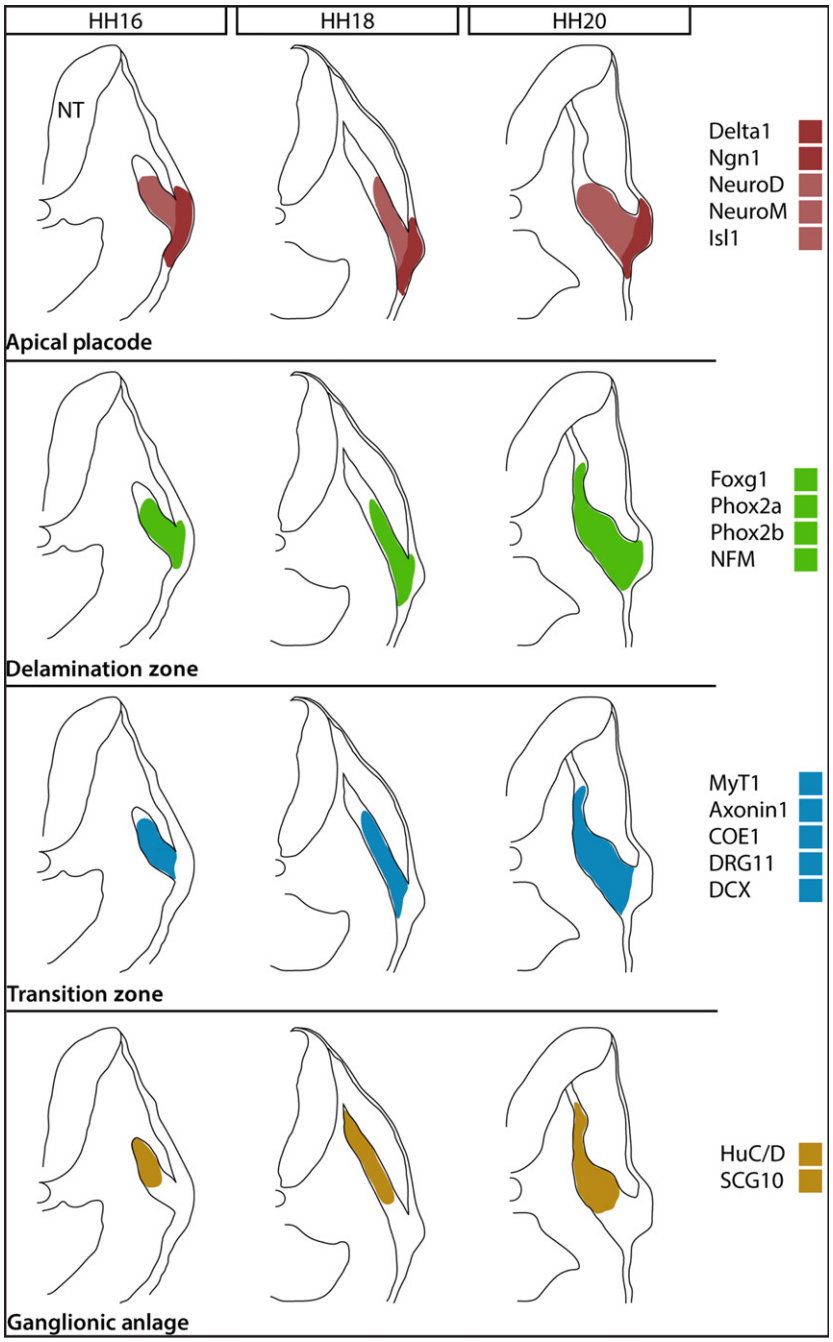

Fig. 8 Schematic representation of the developing petrosal ganglion at the three stages analysed. Black outlines represent the overall morphology of the embryo and migratory stream, while coloured regions represent approximate regions of expression of the four groups of genes identified within the stream. The change in overall morphology of the migratory stream can be seen: at HH16, the stream is made up of a loose cohort of placode-derived cells, extending no further than 60% of the total migratory distance; at HH18, the stream has become more elongated and cohesive, extending to approximately 80% of the total migratory distance; at HH20, a distinct swelling can be seen corresponding to the coalescing ganglion with a narrow stream of cells and neuronal processes extending beyond it towards the neural tube (NT).

1. Initiation at the apical placode: among the panel of markers, *Delta1*, *Ngn1, NeuroD, NeuroM* and *Isl1* were selected as early markers of neurogenesis. These markers showed expression within the placodal ectoderm, spanning the entire width of the epithelium (Figs 3 and 8A). Expression was upregulated within the first 5% of the migratory stream at all stages analysed, suggesting that neurogenesis is initiated at the apical surface of the epithelium. This group could be further subdivided as *NeuroD* and *NeuroM* expres-

sion was maintained in delaminated neuroblasts migrating away from the placode, whereas *Delta1* and *Ngn1* was not.

2. Initiation in the delamination zone: the analysis showed that a second group of markers, *Phox2a, Phox2b, Foxg1* and NFM, was upregulated between 5 and 10% of the migratory stream (Figs 4 and 8B). This relates to the basal region of the placodal ectoderm, where it is difficult to define the basal surface of the epithelium because the basal lamina breaks down at the point of neuroblast exit (Graham et al. 2007). As this region is made up of newborn neuroblasts undergoing delamination from the placodal epithelium, it was suggested that the domain spanning from 5 to 10% of the migratory stream should be termed the delamination zone.
3. Initiation in the transition zone: expression of the third group of markers, *MyT1, Axonin1, CO*E1, *DRG11* and *DCX*, began approximately between 10 and 15% of the migratory stream (Figs 5 and 8C). These markers are thus upregulated in the region of the migratory stream predicted to comprise newly delaminated, early migrating neuroblasts. Thus, it appears that these markers are only turned on once the neuroblasts have left the placodal epithelium and begun migration. It was suggested that this region is a transition zone where neuroblasts upregulate additional neuronal markers while maintaining proliferative potential, and that they migrate through this transition zone as they progress towards the site of ganglionic anlage.
4. Initiation in the ganglionic anlage: the onset of the final group of markers comprising HuC/D and *SCG10* was identified between 15 and 25% of the total migratory distance (Figs 6 and 8D). As HuC/D is a typical marker of post-mitotic neurons (Begbie et al. 2004), this group of markers labels placode-derived neuroblasts that have matured into neurons. The analysis suggests that this occurs as the cells are migrating into the ganglionic anlage.

Comparison of the representative graphs of the expression patterns over time showed that the starting point of expression of each gene was relatively constant across the three developmental stages analysed, placing the markers into the above domains. Qualitative analysis of the images showed that the shape of the migratory stream changes, with a characteristic swelling that was suggested to correspond to the ganglionic anlage (see arrowhead in Figs 3–6). When measured, this region was shown to extend between 25 and 55% of the migratory stream. With the exception of *Delta1* and *Ngn1*, which were restricted to the site of neurogenesis in the placodal epithelium, all of the markers analysed were expressed within this region (Fig. 8).

While the starting point of gene expression was relatively constant across developmental stages, the internal limit of expression along the axis of migration showed more variation (Fig. 8). A trend in the internal limit was observed, with this limit being closer to the NT at each successive stage analysed for the majority of markers. However, *DRG11, NeuroD* and *NeuroM* were notable in that the internal limit of their expression was limited to the ganglionic anlage (white arrowhead in Figs 3C,D and 5C). Other markers were expressed in cells that migrated beyond this point, suggesting that expression of a subset of markers is downregulated once a cell has migrated a certain distance. It is not known what becomes of the cells that migrate past the ganglionic anlage; further study may reveal whether they coalesce back into the ganglion, or whether they die.

Analysis of placodal neuroblast morphology led to the identification of two types of cell morphology: multipolar cells and bipolar cells. The distribution of these cell types within the migratory stream suggests a switch in morphology as the neuroblasts mature (Fig. 7). As such, multipolar cells were first seen at approximately 8% of the migratory stream, corresponding to the delamination zone, suggesting that this is the morphology they assume after losing the cell–cell adhesions holding them within the pseudo-stratified epithelium (Fig. 7E). The bipolar cell morphology was first seen at approximately 25% of the migratory distance, corresponding to the ganglionic anlage (Fig. 7E). Comparison of the graphs for morphology and HuC/D expression showed that the onset of bipolar morphology corresponds with the onset of HuC/D expression (Figs 6Aiv and 7E). While there is some overlap of the multipolar morphology domain into the HuC/D expression domain (Figs 6Aiv and 7E), the qualitative analysis of HuC/D-stained, GFP-electroporated embryos showed that HuC/D-positive cells with multipolar morphology were not observed. The most internal GFP-positive cells were bipolar in morphology and HuC/D-positive, representing differentiated neurons. Thus, it was suggested that the multipolar morphology represents the neuroblast phenotype, and that the neuroblasts switch to the bipolar morphology as they transition into post-mitotic neurons.

The data present a model of sequential neurogenesis through the migratory stream (Fig. 9). The anatomical segregation of the different regions provides a system to examine transitions. Cells are committed to the neuronal fate at the apical surface of the psuedostratified placodal epithelium, where they upregulate *Delta1, Ngn1, NeuroD, NeuroM* and *Isl1*. Apical cells translocate to the basal region of the placodal epithelium where the newly-committed neuroblasts upregulate *Foxg1, Phox2a, Phox2b* and NFM, and delaminate from the epithelium. As neuroblasts begin their migration towards the ganglionic anlage as multipolar cells, they upregulate *Axonin1, COE1, DCX, DRG11* and *MyT1*. As the cells enter the ganglionic anlage they become post-mitotic neurons as opposed to neuroblasts, and start to express HuC/D as well as *SCG10*. The onset of markers of

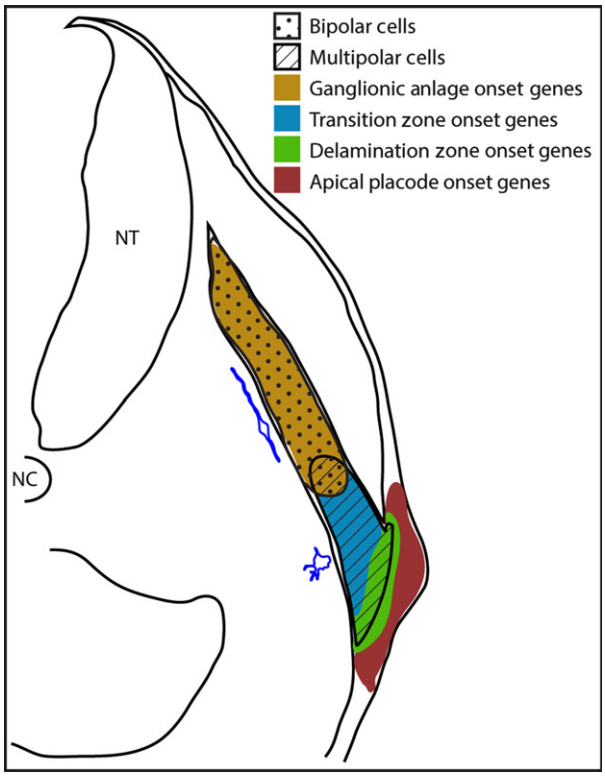

Fig. 9 Representative schematic of the developing petrosal ganglion at HH18. The relative points of gene expression for each of the four groups are shown by the coloured regions. The regions occupied by the multipolar and bipolar cells are shown by hatchings and stipples, respectively. A representative tracing of each morphology type is shown in blue, alongside the region in which they are found. NC, notochord; NT, neural tube.

post-mitotic neurons is also accompanied by a switch to a bipolar morphology (Fig. 9).

That neurogenesis occurs by a sequential process has been demonstrated in other regions of the nervous system (Ratie et al. 2014). Now there is a rigorous description of placodal neurogenesis that can be compared with other examples of neurogenesis. Comparison with NCC sensory neurogenesis at a marker level shows that, while the timing of expression may be different in epibranchial-placode sensory neurogenesis, many of the same neurogenesis genes are used (Marmigere & Ernfors, 2007). Extending this comparison to cell morphology, the switch from multipolar neuroblasts to bipolar neurons described here is reflected by an electron microscope (EM) study of chick DRG development, which showed that within the ganglion there is a small population of less mature multipolar neurons that go through a bipolar stage en route to a mature pseudo-unipolar sensory neuron (Matsuda et al. 1996). Again, however, the timing of these steps differs between the two systems. In the DRG, these changes occur in neurons already in the ganglionic anlage and not in migrating cells, as is the case in the epibranchial ganglia.

Thus, the major difference between CSG and DRG development is in the timing of the deployment of the genetic programme and anatomical segregation of neuronal differentiation. In fact, in this respect, epibranchial placode-derived neuron development resembles cortical neurogenesis. In the cortex expression of a pro-neural bHLH gene (*Ngn* or *Ascl1*) in progenitors located within a pseudostratified epithelium triggers a programme of neuronal differentiation, with neurons maturing as they migrate away from the ventricular zone (Ross et al. 2003). Indeed, during cortical neurogenesis differentiating neuroblasts migrate first as multipolar cells, accumulating in the lower subventricular zone (SVZ) before switching to a bipolar morphology and migrating radially (LoTurco & Bai, 2006). It was hypothesised that the transition zone of the placodes, containing neuroblasts that proliferate and then undergo a multipolar to bipolar transition, may resemble the cortical SVZ. As an initial approach to address this, the transition zone expression of *Tbr2*, a marker of intermediate progenitors in the mouse SVZ, was examined, and found that it was not present. While this specific marker was not expressed, future investigation of gene expression and cellular behaviour may reveal additional parallels between placode transition zone and cortical SVZ.

It is interesting that, unlike the DRG or cortex, mature epibranchial placodal-derived neurons are able to migrate far beyond the internal limit of the ganglionic anlage, with cell bodies located close to the NT. Placodal neuroblasts migrate within a NCC corridor that provides a physical constraint to delineate the pathway for inherent neuroblast migration and axon extension (Freter et al. 2013). It is possible that the neurons close to the NT are early-born pioneer neurons acting within the NCC corridor to provide a scaffold for process extension of later-born cells.

This study demonstrates that placodal sensory neurogenesis can be compared with both sensory neurogenesis from NCC in the trunk, and cortical neurogenesis in the CNS. These comparisons demonstrate similarities and differences to both, suggesting that neurogenesis from the epibranchial placodes occurs via a unique process combining elements from both these well-characterised systems.

Acknowledgements

The authors thank the Anatomical Society for the PhD studentship that supported ACS, and Prof. E. Robertson (Oxford), whose generosity made a third year possible. The authors also thank all their collaborators who have provided them with constructs for *in situ* probes. The authors declare no competing interests.

Author contributions

A.C.S. and J.B. designed experiments and wrote the paper. A.C.S. performed the experiments and analysis. S.J.F. cloned DCX and Tbr2.

References

Abu-Elmagd M, Ishii Y, Cheung M, et al. (2001) cSox3 expression and neurogenesis in the epibranchial placodes. *Dev Biol* **237**, 258–269.

Adameyko I, Lallemend F, Aquino JB, et al. (2009) Schwann cell precursors from nerve innervation are a cellular origin of melanocytes in skin. *Cell* **139**, 366–379.

Alsina B, Abello G, Ulloa E, et al. (2004) FGF signaling is required for determination of otic neuroblasts in the chick embryo. *Dev Biol* **267**, 119–134.

Begbie J (2013) Induction and patterning of neural crest and ectodermal placodes and their derivatives. In: *Comprehensive Developmental Neuroscience: Patterning and Cell Type Specification in the Developing CNS and PNS*. (eds Rubenstein JLR, Rakic P), pp. 239–258. Amsterdam: Academic Press.

Begbie J, Ballivet M, Graham A (2002) Early steps in the production of sensory neurons by the neurogenic placodes. *Mol Cell Neurosci* **21**, 502–511.

Begbie J, Doherty P, Graham A (2004) Cannabinoid receptor, CB1, expression follows neuronal differentiation in the early chick embryo. *J Anat* **205**, 213–218.

Blentic A, Chambers D, Skinner A, et al. (2011) The formation of the cranial ganglia by placodally-derived sensory neuronal precursors. *Mol Cell Neurosci* **46**, 452–459.

Boardman PE, Sanz-Ezquerro J, Overton IM, et al. (2002) A comprehensive collection of chicken cDNAs. *Curr Biol* **12**, 1965–1969.

Capes-Davis A, Tolhurst O, Dunn JM, et al. (2005) Expression of doublecortin (DCX) and doublecortin-like kinase (DCLK) within the developing chick brain. *Dev Dyn* **232**, 457–467.

D'Amico-Martel A, Noden DM (1983) Contributions of placodal and neural crest cells to avian cranial peripheral ganglia. *Am J Anat* **166**, 445–468.

Englund C, Fink A, Lau C, et al. (2005) Pax6, Tbr2, and Tbr1 are expressed sequentially by radial glia, intermediate progenitor cells, and postmitotic neurons in developing neocortex. *J Neurosci* **25**, 247–251.

Freter S, Fleenor SJ, Freter R, et al. (2013) Cranial neural crest cells form corridors prefiguring sensory neuroblast migration. *Development* **140**, 3595–3600.

Garcia-Dominguez M, Poquet C, Garel S, et al. (2003) Ebf gene function is required for coupling neuronal differentiation and cell cycle exit. *Development* **130**, 6013–6025.

George L, Kasemeier-Kulesa J, Nelson BR, et al. (2010) Patterned assembly and neurogenesis in the chick dorsal root ganglion. *J Comp Neurol* **518**, 405–422.

Graham A, Blentic A, Duque S, et al. (2007) Delamination of cells from neurogenic placodes does not involve an epithelial-to-mesenchymal transition. *Development* **134**, 4141–4145.

Groves AK, George KM, Tissier-Seta JP, et al. (1995) Differential regulation of transcription factor gene expression and phenotypic markers in developing sympathetic neurons. *Development* **121**, 887–901.

Hamburger V, Hamilton HL (1992) A series of normal stages in the development of the chick embryo, 1951. *Dev Dyn* **195**, 231–272.

Hatini V, Ye X, Balas G, et al. (1999) Dynamics of placodal lineage development revealed by targeted transgene expression. *Dev Dyn* **215**, 332–343.

Kitazawa A, Kubo K, Hayashi K, et al. (2014) Hippocampal pyramidal neurons switch from a multipolar migration mode to a novel "climbing" migration mode during development. *J Neurosci* **34**, 1115–1126.

Ladher RK, O'Neill P, Begbie J (2010) From shared lineage to distinct functions: the development of the inner ear and epibranchial placodes. *Development* **137**, 1777–1785.

Lassiter RN, Stark MR, Zhao T, et al. (2014) Signaling mechanisms controlling cranial placode neurogenesis and delamination. *Dev Biol* **389**, 39–49.

LoTurco JJ, Bai J (2006) The multipolar stage and disruptions in neuronal migration. *Trends Neurosci* **29**, 407–413.

Marmigere F, Ernfors P (2007) Specification and connectivity of neuronal subtypes in the sensory lineage. *Nat Rev Neurosci* **8**, 114–127.

Matsuda S, Baluk P, Shimizu D, et al. (1996) Dorsal root ganglion neuron development in chick and rat. *Anat Embryol (Berl)* **193**, 475–480.

Matsushita F, Kameyama T, Marunouchi T (2002) NZF-2b is a novel predominant form of mouse NZF-2/MyT1, expressed in differentiated neurons especially at higher levels in newly generated ones. *Mech Dev* **118**, 209–213.

McCabe KL, Sechrist JW, Bronner-Fraser M (2009) Birth of ophthalmic trigeminal neurons initiates early in the placodal ectoderm. *J Comp Neurol* **514**, 161–173.

Neukirchen D, Bradke F (2011) Neuronal polarization and the cytoskeleton. *Semin Cell Dev Biol* **22**, 825–833.

Niederlander C, Lumsden A (1996) Late emigrating neural crest cells migrate specifically to the exit points of cranial branchiomotor nerves. *Development* **122**, 2367–2374.

Parras CM, Schuurmans C, Scardigli R, et al. (2002) Divergent functions of the proneural genes Mash1 and Ngn2 in the specification of neuronal subtype identity. *Genes Dev* **16**, 324–338.

Perrot R, Berges R, Bocquet A, et al. (2008) Review of the multiple aspects of neurofilament functions, and their possible contribution to neurodegeneration. *Mol Neurobiol* **38**, 27–65.

Ratie L, Ware M, Jagline H, et al. (2014) Dynamic expression of Notch-dependent neurogenic markers in the chick embryonic nervous system. *Front Neuroanat* **8**, 158.

Rebelo S, Reguenga C, Osorio L, et al. (2007) DRG11 immunohistochemical expression during embryonic development in the mouse. *Dev Dyn* **236**, 2653–2660.

Ross SE, Greenberg ME, Stiles CD (2003) Basic helix-loop-helix factors in cortical development. *Neuron* **39**, 13–25.

Sessa A, Mao CA, Colasante G, et al. (2010) Tbr2-positive intermediate (basal) neuronal progenitors safeguard cerebral cortex expansion by controlling amplification of pallial glutamatergic neurons and attraction of subpallial GABAergic interneurons. *Genes Dev* **24**, 1816–1826.

Tabata H, Kanatani S, Nakajima K (2009) Differences of migratory behavior between direct progeny of apical progenitors and basal progenitors in the developing cerebral cortex. *Cereb Cortex* **19**, 2092–2105.

Thompson H, Blentic A, Watson S, et al. (2010) The formation of the superior and jugular ganglia: insights into the generation of sensory neurons by the neural crest. *Dev Dyn* **239**, 439–445.